International Journal of Pavement Engineering
Vol. 9, No. 6, December 2008, 413–429

Taylor & Francis
Taylor & Francis Group

Evaluation of geogrids for stabilising weak pavement subgrade

Xiaochao Tang[1], Ghassan R. Chehab* and Angelica Palomino[2]

Department of Civil and Environmental Engineering, The Pennsylvania State University, University Park, PA, USA

(*Received 24 February 2008; final version received 7 June 2008*)

This study attempts to identify mechanical and physical properties of geogrids that are critical to their effectiveness in the stabilisation of pavement subgrade. Geogrid properties, including aperture size, wide-width tensile strength and junction strength, for four geogrid products are correlated with bench-scale interface test results, including direct shear and pull-out, and accelerated pavement testing (APT) results. APT is conducted through the use of a one-third scale APT device, the model mobile load simulator (MMLS3) on geogrid-reinforced pavement sections. The pavement sections are constructed on a subgrade soil with a low California bearing ratio. The performance of each pavement section is evaluated by measuring surface rutting at various trafficking stages. The analysis reveals a strong relationship between performance and junction and tensile strength of geogrids at small strains, whereas aperture size has a positive correlation with pull-out test results.

Keywords: geogrid; subgrade stabilisation; pavement; bench-scale testing; accelerated testing, MMLS3

1. Introduction

Geogrids have been widely used as reinforcement in structures with unbound materials, such as pavements, slopes, retaining walls and embankments. It has been shown that, in a pavement system, the inclusion of geogrids at the interface between a pavement base course and subgrade can significantly improve the performance of the pavement on a weak subgrade according to both laboratory tests and full-scale field experiments (Barksdale *et al.* 1989, Al-Qadi *et al.* 1994, 2007, Perkins 1999, Hufenus *et al.* 2006). Given a proper ratio of geogrid aperture size to aggregate grain size, geogrids provide lateral confinement to the pavement aggregate base course (ABC) through shear resistance and friction between the geogrid and surrounding aggregate. The confinement due to the geogrid increases the modulus of the aggregate, which leads to an improved vertical stress distribution over the subgrade and consequent reduction in vertical subgrade deformation (Love 1984, Hass *et al.* 1988). Reduction in deformation also results from reduction in shear stress transfer at the geogrid–subgrade interface (Perkins 1999). Additional types and mechanisms of reinforcement – surface friction along the geogrid, passive thrust against the geogrid's bearing ribs, aggregate interlocking between the apertures, and/or soil–soil friction – are mobilised by the presence of geogrids depending on the application and type of environmental and loading conditions (Shukla 2002).

The effectiveness of geogrid reinforcement is highly dependent on physical and mechanical properties, i.e. index properties, of the geogrid and on the properties of the interface between the geogrid and the surrounding materials. Results from direct shear and pull-out tests are the most commonly used parameters depicting the soil–geogrid interaction characteristics. Characteristics identified through those tests are a function of the geogrid material mechanical properties, shape and texture, as well as soil and aggregate properties, such as gradation, plasticity, density and moisture content, applied normal stress and loading rate (Ingold 1983, Jewell *et al.* 1984, Farrag *et al.* 1993).

Identification of geogrid properties critical for optimising the effectiveness of a specific reinforcement mechanism can be achieved by correlating the known geogrid properties, e.g. junction strength, with the response of geogrids in bench-scale interface tests and model-scale performance tests. Accelerated pavement testing (APT) has been used successfully for evaluating geogrid performance for pavement applications in the USA since 1909 (Metcalf 1996). The advantages of APT are the ability to conduct performance tests at relatively low costs over a short time period, and the ability to control the loading and environmental conditions.

This study focuses on correlating the index properties of geogrids with the results of bench-scale testing and accelerated testing. Testing includes standard index property tests, interface tests, including direct shear and pull-out tests and APT. An in-depth analysis is then conducted to correlate the values of index properties with the results of bench-scale testing and performance-based APT. Through the correlation analysis, the geogrid index properties that most influence the performance of geogrids as a means for flexible pavement subgrade stabilisation are identified.

*Corresponding author. Email: gchehab@engr.psu.edu

ISSN 1029-8436 print/ISSN 1477-268X online

DOI: 10.1080/10298430802279827
http://www.informaworld.com

2. Experimental design

2.1 Materials

2.1.1 Geogrids

Four commonly used biaxial geogrid products are selected for this study and are herein designated as Grids A–D. Grids A and D are composed of high tenacity polyester multifilament yarns and coated with a proprietary polymer and polyvinyl chloride coating, respectively. Grid B is made of woven polypropylene (PP) yarns, while Grid C is made of extruded PP sheets. Based on the measured flexural rigidity as per ASTM D1388, Grids A, B and D are classified as flexible geogrids, while Grid C is classified as a stiff geogrid (Koerner 1998).

2.1.2 Subgrade soil

The subgrade material is a silty sand. Table 1 provides a summary of the subgrade soil properties. The soil grain size distribution is shown in Figure 1. The soil is classified as SW-SM, which is a well-graded silty sand in accordance with ASTM D2487 and A-2-4(0) in accordance with AASHTO M145.

Table 1. Subgrade soil properties.

Property	Measurement methods	Result
Classification	AASHTO M145/ ASTM D2487	A-2-4(0)/SW-SM
Per cent passing #200 sieve (%)	ASTM D422	6.2
Liquid limit (%)	ASTM D4318	17.6
Plastic limit (%)	ASTM D4318	14.7
Optimum moisture content (%)	ASTM D698	10.0
Maximum dry density (kg/m^3)	ASTM D698	2066
Friction angle, ϕ (deg)	ASTM D3080	31.8

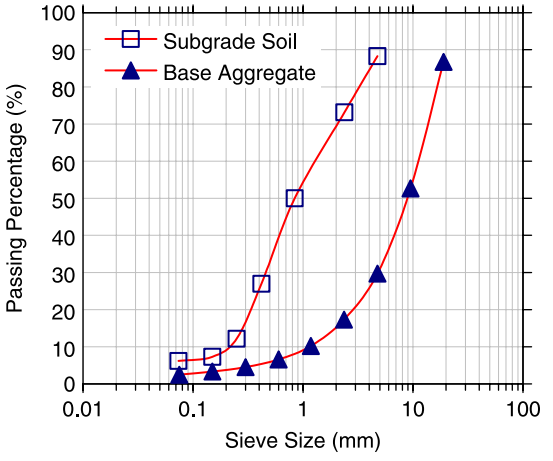

Figure 1. Grain size distribution of subgrade soil and base course aggregates.

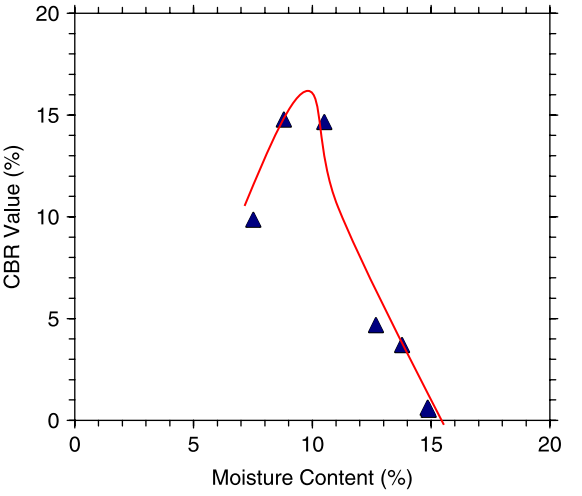

Figure 2. CBR variation with water content for the subgrade soil.

A set of laboratory unsoaked California bearing ratio (CBR) tests (ASTM D1188) are performed on the soil at different water contents, as shown in Figure 2. CBR decreases significantly with an increase in water content beyond the optimum water content (10%), indicating the soil is water sensitive. Hence, the soil is compacted at a water content greater than optimum to induce weak soil conditions.

2.1.3 Base course aggregate

Dense-graded crushed stone is used for the pavement ABC layer. A standard Proctor test for the aggregates yields an optimum moisture content of 3.9% and maximum dry density of 2329 kg/m^3.

2.1.4 Hot mix asphalt

The asphalt mixture is provided by a local hot mix asphalt plant. The asphalt mixture has a theoretical maximum specific gravity of 2.510. No laboratory tests are conducted for asphalt mixture properties since the same asphalt concrete (AC) layer is used for all sections and thus is not considered a variable in this study. Air voids (AVs) of the constructed asphalt layer are measured as they are pertinent to overall pavement deformation as discussed in subsequent sections.

3. Experimental tests

3.1 Index tests

Index tests are performed on the four biaxial geogrid products to determine their physical and mechanical properties. Testing was conducted following ASTM

Table 2. Tested index properties of the geogrids (Chehab *et al.* 2007).

		Geogrid							
		Grid A		Grid B		Grid C		Grid D	
Index property	Test method	MD*	TD**	MD	TD	MD	TD	MD	TD
Aperture size (mm)	Calipers	27.18	28.96	35.05	41.15	25.65	36.58	25.65	26.42
Rib thickness (mm)	Calipers	0.76	1.12	1.98	1.09	0.76	1.07	1.42	2.03
Junction thickness (mm)	ASTM D5199	1.17		2.29		3.94		1.55	
Mass per unit area (g/m^2)	ASTM D5261	298.37		252.26		319.06		350.93	
Tensile strength at 2% strain (kN/m)		7.5	10.1	14.8	15.0	9.8	15.6	10.3	11.2
Tensile strength at 5% strain (kN/m)	ASTM D6637	13.1	14.1	30.1	30.0	16.8	29.2	18.1	17.4
Ultimate tensile strength (kN/m)		33.3	57.8	36.5	35.7	23.9	32.9	39.5	52.8
Elongation at break (%)		10.5	14.0	7.1	6.7	20.6	10.9	10.5	12.0
Junction strength (kN/m)	GRI GG2	6.1	7.6	10.2	4.3	17.7	28.1	7.4	7.1
Flexural rigidity (mg cm)	ASTM D1388, modified	146,119		271,509		1,429,355		452,671	
Torsional stiffness (cm kg/deg)	COE/GRI GG9	3.47		3.97		7.50		3.43	

*MD, machine direction; **TD, transverse/cross-machine direction.

standards as well as standards set forth by the Geosynthetic Research Institute (GRI). Properties measured from index tests are the most commonly used criteria in specifications for use of geogrid products by state highway agencies. Table 2 lists the index tests conducted on the four geogrid products, standard test protocols followed, along with the measured values of physical and mechanical properties.

3.2 Bench-scale tests

The objective of the bench-scale tests is to evaluate the performance of the geogrid under the conditions and in the medium in which it will be installed, as opposed to index tests where the geogrid is tested in isolation. Direct shear and pull-out tests are conducted in this study to characterise the interaction properties of the various types of geogrids installed between the subgrade and the aggregates used in the aggregate base layer.

3.2.1 Direct shear test

The direct shear test is conducted in conformance with ASTM D3080 to measure the friction angle and adhesion at the interface between the subgrade and the aggregate base layer, with and without a geogrid in place. The soil, aggregate and geogrid products of the test specimens are the same as those used in the APT. The geogrids are placed between the upper aggregate box and the lower soil box. The dimensions of both the boxes are 5.1 cm × 30.5 cm × 10.2 cm. The base aggregate is remoulded and compacted to 100% of maximum dry density at optimum moisture content. The subgrade soil for these tests is compacted to 92.5% of maximum dry density at optimum moisture content (10%). Direct shear tests are performed under three different normal pressures: 12, 27 and 36 kN/m^2. The selected pressure of 27 kN/m^2 is an estimate of the pressure imparted on the pavement subgrade during the APT based on the applied traffic loading. Shear forces are applied at a constant displacement rate of 0.1 cm/min, slow enough to dissipate soil pore pressure.

Figure 3(a) shows the direct shear test results for the control interface, i.e. subgrade soil–base aggregates without geogrids. The shear stresses at zero displacement indicate the resistance to sliding. As expected, the applied shear stress increases with increasing normal pressure. The shear strength parameters of the interface, adhesion and friction angle, can be obtained from the Mohr–Coulomb failure envelope derived from the peak values of direct shear test results (Figure 3(b)).

Given the shear strength parameters of the control interface, the interface efficiency factor can be calculated as (Koerner 1998)

$$E_\phi = \frac{\tan\delta}{\tan\phi}, \tag{1}$$

where δ is the friction angle of the geogrid reinforcement interface and ϕ is the friction angle of the control interface. The efficiency factor for geotextiles varies from 0.6 to 1, but can be greater than 1 for geogrids (Juran *et al.* 1988). Table 3 provides a summary of the tested properties from direct shear tests for the geogrid-reinforced interfaces. The four tested geogrids have interface efficiency factors greater than 0.5.

Figure 4 illustrates the shear stress–displacement behaviours for the geogrid-reinforced soil–aggregate interfaces under the same normal pressure of 27 kN/m^2. Although, the interface characteristics during direct shear tests can be influenced by many factors, such as applied normal pressure, geogrid material characteristics and drainage conditions, for this study, the geogrid material properties are expected to be the only factor affecting the

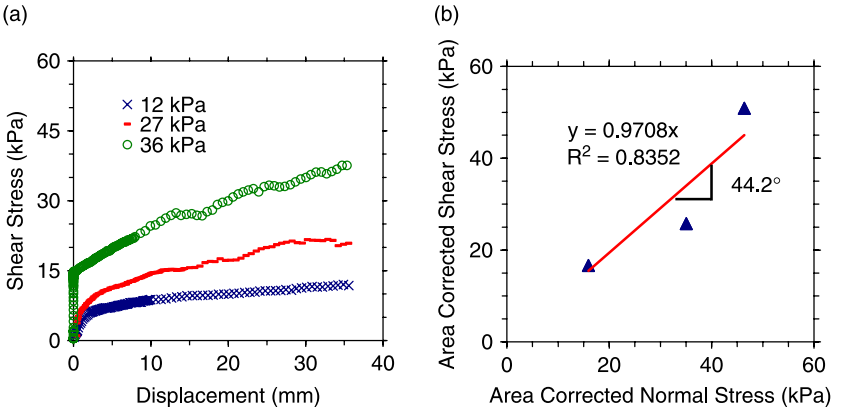

Figure 3. Direct shear tests: (a) shear stress–displacement under three normal pressures and (b) friction angle of the control interface.

interface since all other factors are held constant among the four tests.

3.2.2 *Pull-out test*

Pull-out tests are conducted on four geogrids in a medium consisting of the base course aggregates used in the pavement section as per ASTM D6706 in the machine direction of the geogrid. The pull-out test set-up is shown in Figure 5. The geogrid samples are cut into 1.2 m × 0.6 m sections and inserted into a 0.4 m thick compacted aggregate layer with the machine direction ribs oriented parallel to the pull-out direction. All pull-out tests are carried out under a normal pressure of 6.9 kN/m^2 and at a displacement rate of 0.1 cm/min. The geogrid displacements are measured at the front and at 31, 61, 89 and 116 cm away from the front through a telltale system having steel wires connecting geogrids to linear variable differential transformers.

Table 3. Results of the direct shear and pull-out tests.

Property	Grid A	Grid B	Grid C	Grid D	Control
Friction angle, δ_{peak} (deg)	28.6	44.0	48.0	32.7	44.2
Efficiency factor, E_ϕ	0.56	0.99	1.14	0.66	N/A
Adhesion, c (kN/m^2)	1.72	0.00	0.00	3.69	0
Interaction coefficient, C_i	0.86	1.00	0.82	0.62	N/A

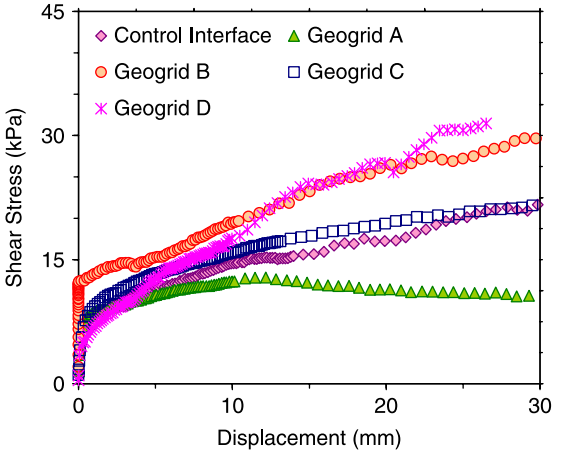

Figure 4. Shear stress–displacement at the subgrade–aggregate base interface under a pressure of 27 kN/m^2 for the control case and with each of the four tested geogrids.

The interaction coefficient, C_i, represents the ratio of the average interface strength to the internal shear strength of the base course aggregates and is used herein to quantify the reinforcement effectiveness for pull-out tests. C_i is calculated according to Bergado and Chai (1994) and Tatlisoz *et al.* (1998) as

$$C_i = \frac{P}{2\,WL(c + \sigma_n \tan\phi)}, \qquad (2)$$

where C_i is the coefficient of interaction, P is the maximum pull-out load, σ_n is the applied normal pressure, c is the adhesion of soil medium tested, ϕ is the friction angle of soil medium tested, W is the width of the geogrid specimen and L is the embedded length of the geogrid in the soil.

C_i is a function of frictional characteristics between the geogrids and the surrounding unbound materials, the strength of the geogrid junctions, the flexural stiffness of the transverse ribs and the geogrid per cent open area. The calculated interaction coefficients for the four geogrid cases are presented in Table 3. A strong bond between the soil and the geogrid corresponds to an interaction coefficient value greater than 1. An interaction coefficient less than 0.5 implies a weak bond between the geogrid and the surrounding materials and/or possible breakage of geogrid cells. Most values reported for geosynthetics range between 0.5 and 1 (Mohiuddin 2003).

Figure 6 shows the pull-out force–displacement relationships for Grids A–D at the nearest location

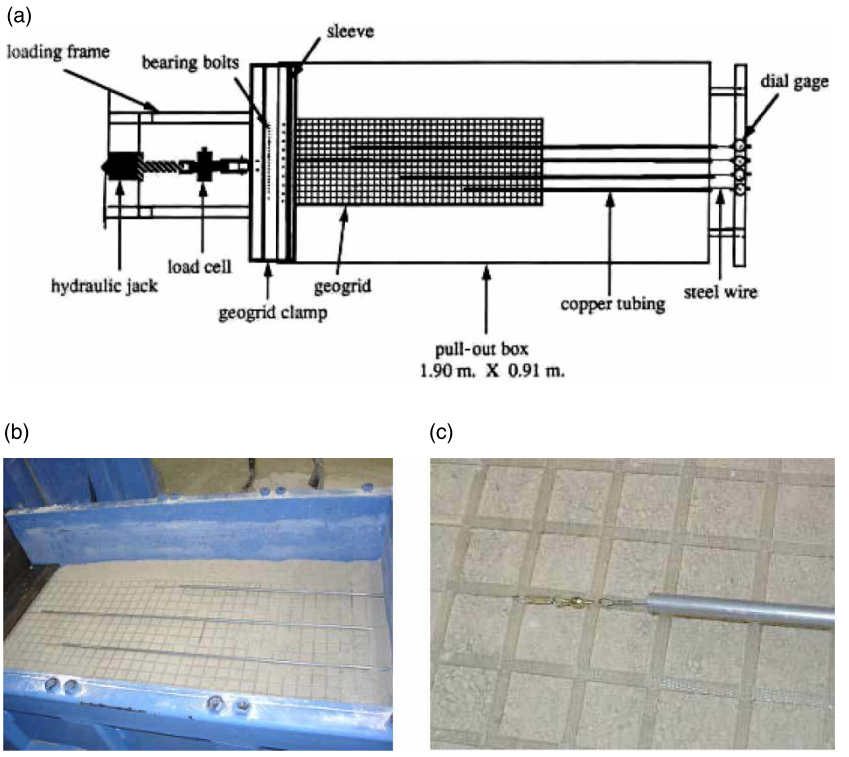

Figure 5. Pull-out test set-up: (a) schematic plan view of the pull-out box; (b) top view of the pull-out box showing the geogrids on the soil and tubes housing steel wires and (c) connection of steel wire to a geogrid rib (courtesy by TRI Inc.).

(31 cm) from the front face of the pull-out box. Grid B exhibits the highest peak pull-out force. Although, Grid C's interaction coefficient, derived from the maximum pull-out load, is the second lowest among the four geogrids, Grid C has the best pull-out resistance at small displacements (up to 11 mm in this case). Similar trends are observed at the other locations: 61, 89 and 116 cm from the front face. Note that the attributes of geogrids at small strains are important when geogrids are used as pavement reinforcement since traffic-induced deformation of geogrids in pavements is minimal. From that standpoint, the coefficient of interaction results should be used cautiously. The magnitude of the necessary pull-out force to induce small displacements is more indicative of performance in pavements.

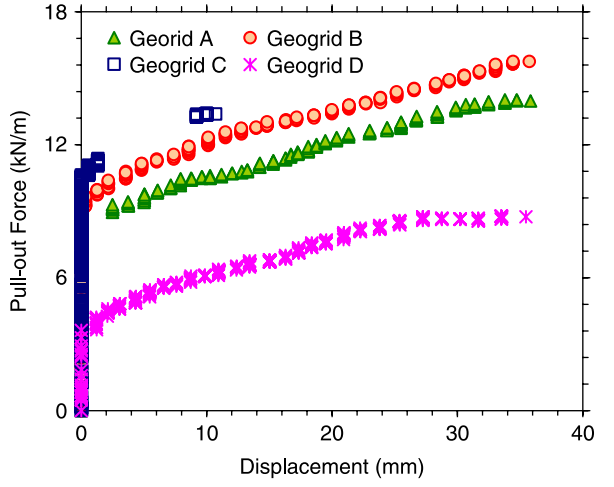

Figure 6. Pull-out load–displacement for Geogrids A–D at locations 31 cm from the front of the pull-out box.

Figure 7 demonstrates the relationship between the pull-out force and the displacement at different distances from the front of the pull-out box for Grids C and D, which represent stiff and flexible geogrid behaviours, respectively. Along the pull-out direction, the portion of Grid C furthest from the pulled end (back end of the pull-out box) does not show significant movement until the occurrence of pull-out failure. By contrast, significant displacement at all the telltale locations indicates possible slippage of Grid D at the interface. This again indicates that Grid C has better pull-out resistance in spite of its low interaction coefficient.

3.3 *Accelerated pavement testing*

Accelerated testing is conducted on laboratory-fabricated slabs for the four types of geogrid products using the one-third scale model mobile load simulator (MMLS3). Two sets of accelerated pavement tests are performed, each for a different subgrade CBR value. The first set of testing, denoted as APT I, corresponds to the testing of all four geogrids on a subgrade with a CBR value of 3, while the

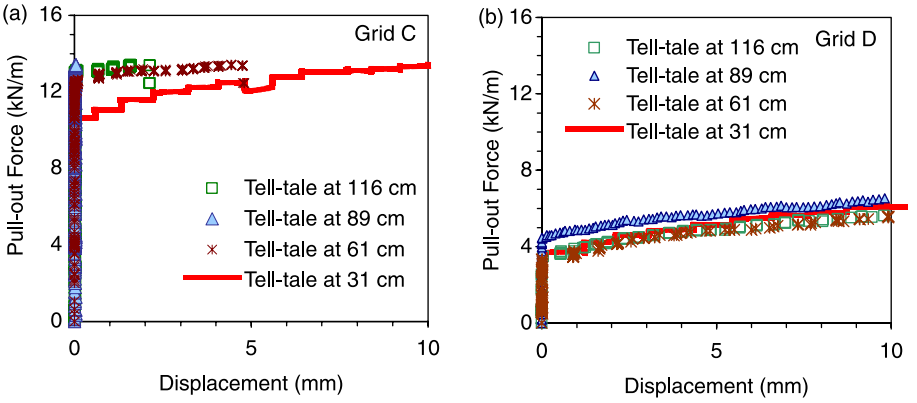

Figure 7. Relationship between the pull-out force and the displacement: (a) Geogrid C and (b) Geogrid D.

subgrade for the second set of testing (APT II) has a CBR value of 1.5. Only three of the four geogrids are tested in APT II: Grids B–D, in addition to a control section with no geogrid.

3.3.1 *Testing equipment*

The MMLS3, as shown in Figure 8, is an APT device that applies unidirectional trafficking to the pavement in a controlled laboratory environment or on full-scale pavements in the field.

The MMLS3 has four tyres, each with a diameter of 30 cm and a width of 8 cm. The actual wheel path generated by the MMLS3 is approximately 137 cm long. The load exerted by each wheel of the MMLS3 is 2.7 kN, with a corresponding tyre pressure of 621 kPa. The MMLS3 suspension system is designed so that the wheel load is independent of the wheel vertical displacement; thus, the applied load remains constant even if rutting occurs. The traffic speed is set to 7200 axles (wheels) per hour or two axles (wheels) per second. Testing is conducted at room temperature under dry conditions with no wandering, i.e. channelised trafficking.

The P900 contact-type electronic profilometer (MLS Test Systems Pty Ltd, Stellenbosch, South Africa) is used to measure pavement rutting profiles. Measurements are made through a 25 mm diameter, 10 mm wide steel wheel that rolls on the pavement surface. The vertical measurement resolution is approximately 1 μm and the repeatability is in the range of 10 μm. The maximum vertical displacement that can be measured is 40 mm. The increment of the measuring wheel is 2 mm; that is, profile measurements are recorded every 2 mm across the wheel path.

In accordance with ASTM D7113, a non-nuclear density gage, Pavement Quality Indicator™ (PQI) Model 301 (Engius, LLC), is used to provide quick readings of density, temperature and moisture content of the AC layer. The PQI works through a constant voltage, low frequency and electrical impedance mechanisms.

3.3.2 *Pavement slabs*

3.3.2.1 Configuration. The pavement slabs are constructed in a test pit with reinforced concrete walls and foundations. The pit is backfilled with aggregate base and compacted to serve as pavement bedrock. Figure 9 shows the layout of the constructed pavement sections for APT I. There are four constructed sections labelled R1, R2, R3 and R4 that are reinforced with Geogrids A–D, respectively. Similarly, four pavement sections, P1–P4, are constructed for APT II. Section P1 is a control section, i.e. no geogrid, while sections P2, P3 and P4 are reinforced with Geogrids B, C and D, respectively. The four pavement slabs are constructed using the same materials for the individual layers. The subgrade is placed on top of a waterproof membrane to avoid moisture loss to the bedrock layer below. Subgrade soil and ABC are placed and compacted uniformly and at the same moisture content for all sections. The only difference among the sections is the geogrid type at the subgrade–ABC interface.

3.3.2.2 Structure. The MMLS3 applies a wheel load of 2.7 kN with a contact pressure of 690 kPa (100 psi) roughly representing one-ninth of the loading conditions applied by a standard full-scale single tyre (one-quarter dual-tyre ESAL). In an effort to attain similitude between the scaled slabs and the actual field slabs, the thickness of each layer should be scaled approximately to one-third of that in the field (Martin *et al.* 2003).

In this study, the Kenlayer program (Huang 2004) is used to determine the required scaling ratio that is expected to be close to 1/3. The thicknesses of AC and base course layers of 3.8 cm (1.5 in.) and 7.6 cm (3 in.), respectively, are found to lead to vertical stresses on top of the subgrade and horizontal strains in the geogrid similar to those for typical full-scale flexible pavements comprising 10 cm of AC and 20 cm ABC. This corresponds to a scaling ratio of 1/2.6.

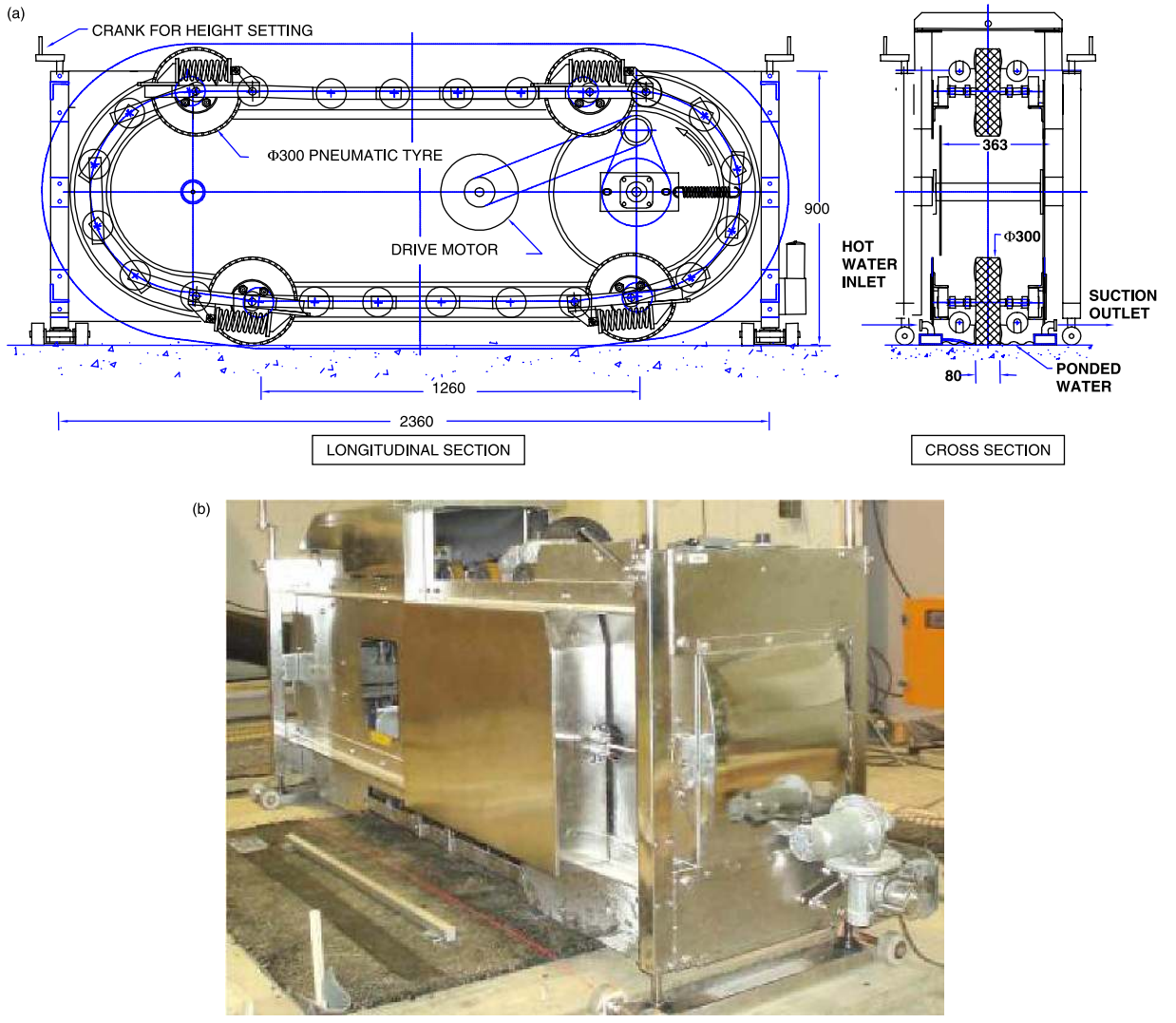

Figure 8. One-third scale MMLS3: (a) schematic, units in mm and (b) MMLS3 mounted on top of a laboratory pavement slab.

3.3.2.3 Construction. The pavement subgrade soil is compacted in three lifts with a vibratory plate compactor. The compactor travel direction ensures consistency of the soil density throughout the pit. The geogrids are carefully unrolled to avoid folds and wrinkles and placed directly on the subgrade layer. The geogrids from adjacent sections have a 7.6 cm overlap to ensure adequate development length, and the ends of the geogrid sections are folded against the pit walls to obtain necessary anchorage and slight pre-tensioning, as well as to prevent shifting of the geogrids out of position (Figure 9). The geogrid is overlaid with an ABC layer compacted using a vibratory plate compactor. A 6% AV content is targeted for the AC layer. The target AV is similar to that targeted in field construction and is expected not to significantly contribute to the overall rutting of the pavement, since the low CBR of the subgrade would lead to extensive deformation that dominates the overall pavement rutting. Table 4 presents the as-constructed layer properties for both APTs I and II.

The AC layer density is measured along the wheel path for each section using the PQI non-nuclear density gage prior to MMLS3 trafficking. Figure 10 presents a contour plot of the measured AV distribution for each section measured after construction and before trafficking. The asphalt layer in sections R3 and P3 reinforced by Grid C has significantly higher AVs than the other sections in both test sets. It is highly likely that the high AC AVs in these two sections result from the attributes of the geogrid itself, which has a significantly higher stiffness than the other geogrids tested, given the uniform compaction technique and consistent pavement structure and materials used. Further studies that incorporate different types of geogrids and subgrade soils are needed to confirm and further understand the mechanisms causing this phenomenon.

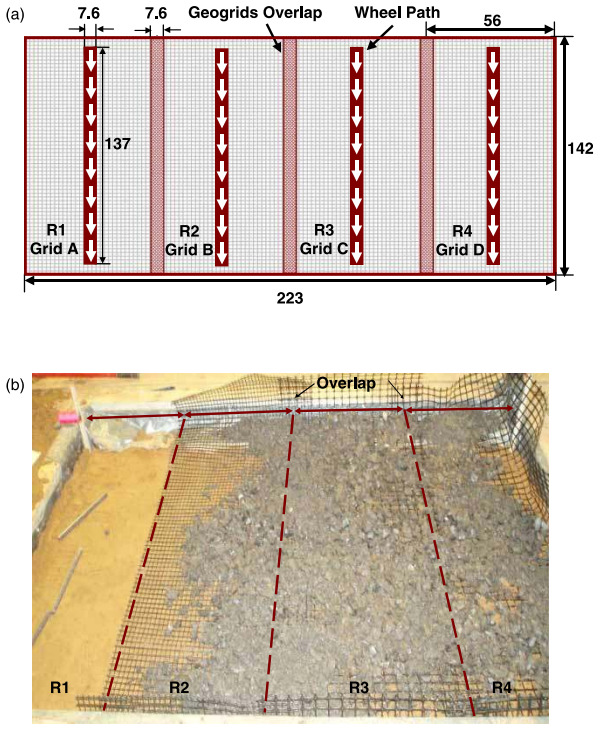

Figure 9. Pavement section layout: (a) dimensions, units in cm and (b) plan view of the section and geogrid installation.

3.3.3 *Accelerated trafficking of slabs*

3.3.3.1 APT I. A total of 140,000 MMLS3 traffic cycles are applied to each section. Rutting accumulation at specific locations throughout each section is measured and averaged. Figure 11(a) shows the rutted wheel path for each section. To shed light on the accumulation of deformation as trafficking cycles are applied, the measured rutting profile for section R3 at various traffic cycles is also plotted in Figure 11(c).

3.3.3.2 APT II. Rutting failure in the APT II test sections occurs well before 140,000 MMLS3 traffic cycles can be applied. Hence, MMLS3 trafficking is applied to each section of the APT II slab until rutting failure occurs. The control section P1 exhibits extensive deformation after 40,000 wheel applications, while similar deformation is observed at 70,000 applications for section P2. Trafficking is stopped at 100,000 wheel applications for sections P3 and P4. Figure 11(b) shows the rutted wheel paths for the fours sections. The extensive rutting and resulting cracking at the edge of the wheel path for the control section P1 is clearly visible. The measured rutting profile for section P3 is also shown in Figure 11(d).

4. Observations and analysis of results

Except for the difference in geogrid products, the experimental variables are minimised as much as possible in the bench-scale testing and APT. The subgrade soil, ABC and asphalt materials are consistent for all tests. It is therefore reasonable to presume that most of the difference in the performance is due to the intrinsic properties of geogrids and their interaction characteristics with the medium in which they are placed. This section first covers the observation and analysis of the performance of the geogrids from accelerated trafficking. An attempt is then made to find possible correlations among physical and mechanical properties of geogrids (index properties), mechanistic parameters from bench-scale testing and performance from accelerated testing of the scaled slabs. The comparisons conducted are limited to particular index

Table 4. As-constructed pavement layer properties.

APT	Subgrade thickness (cm)	Base course thickness (cm)	AC thickness (cm)	Subgrade moisture content (%)	Subgrade CBR value (%)
I	23.6	6.6	3.8	14	3
II	15.2	6.6	3.8	14.8	1.5

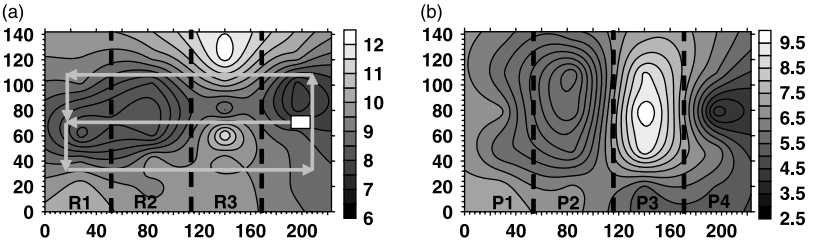

Figure 10. AV content distribution in the asphalt layer: arrows represent compaction path (same for both test sets) and shading represents the range of AV content: (a) APT I and (b) APT II.

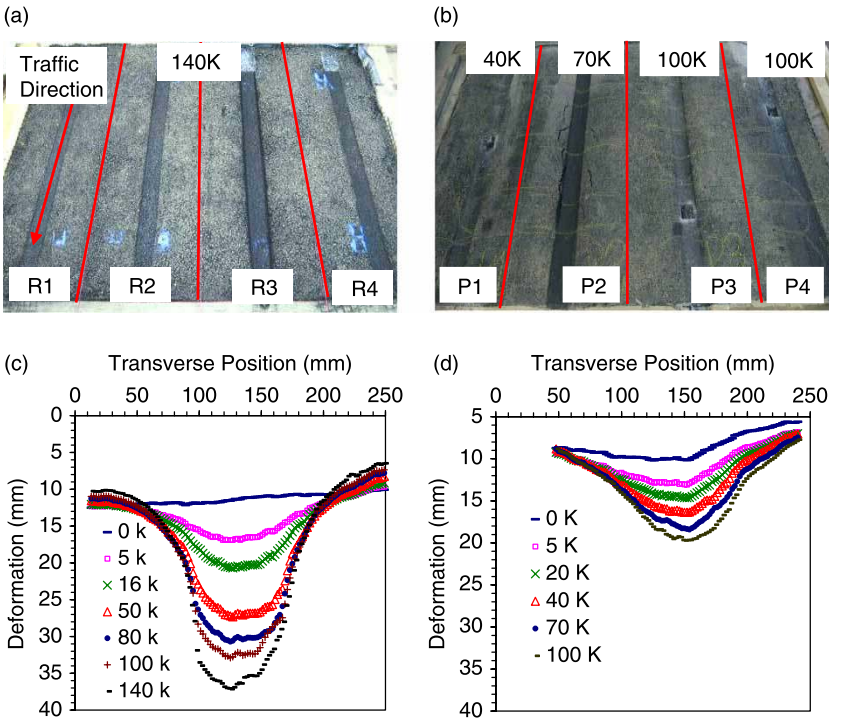

Figure 11. Rutting of the wheel paths: (a) APT I and (b) APT II; measured rutting profile at various stages of trafficking for sections: (c) R3 in APT I and (d) P3 in APT II based on the average from all measured locations along the wheel path.

properties that are deemed important for pavement applications, i.e. low strain conditions.

4.1 Performance of geogrids – accelerated testing

4.1.1 APT I

In APT I, the most significant rutting is observed for section R3 (Grid C), as shown in Figure 12(a). However, this could partially be attributed to the high AV of the AC layer and the possible densification of that layer (Figure 10(a)). By comparing the other three sections R1, R2 and R4 which had relatively similar AV, it is evident that Grids A and B exhibit similar rutting for this type of subgrade soil, with higher rutting in section R4 reinforced with Grid D.

After trafficking, the slab is trenched across the travel direction to expose the pavement cross-section. Figure 13 shows extensive densification occurred in the AC layer of section R3 with minimal densification occurring in R4. A significant amount of soil slurry is observed underneath the wheel path at the geogrid–aggregate base interface, probably due to soil pumping from the subgrade into the aggregate base layer during traffic loading.

4.1.2 APT II

The control section P1 exhibits significantly higher rutting that accumulated relatively quickly (failure occurs at 40,000 cycles) compared to the reinforced sections (failure between 70,000 and 100,000 cycles). This illustrates the ability of geogrids to stabilise weak subgrade and potential to minimise pavement deformation under the traffic load. Similar to APT I, section P3 reinforced with Geogrid C exhibits relatively higher rutting among the reinforced sections, probably due to the higher AVs and consequent rutting of the AC layer (Figure 12(b)).

In order to minimise the effect of variation in the AV content of the asphalt layer, the rutting accumulation at locations with similar compacted asphalt AVs is presented in Figure 12(c). Section P2 (Grid B) has the second highest cumulative rutting among the four test sections. The rate of rutting accumulation for sections P1 and P2 is slightly higher than that for sections P3 and P4. Significantly higher rutting is observed for section P4 (Grid D) when compared to that for P3 (Grid C). Overall, the relatively stiffer geogrid, Grid C, shows the best performance with respect to the rutting resistance for the tested pavement on this specific weak subgrade.

4.1.3 Comparison between APTs I and II

The significant variable in designing the sections of APTs I and II is the subgrade CBR, with a subgrade CBR of 3 and 1.5 for APTs I and II, respectively. The ranking of the geogrid products in terms of the ability to minimise subgrade rutting is somewhat different between APTs I and II. One noticeable difference is the switch in ranking

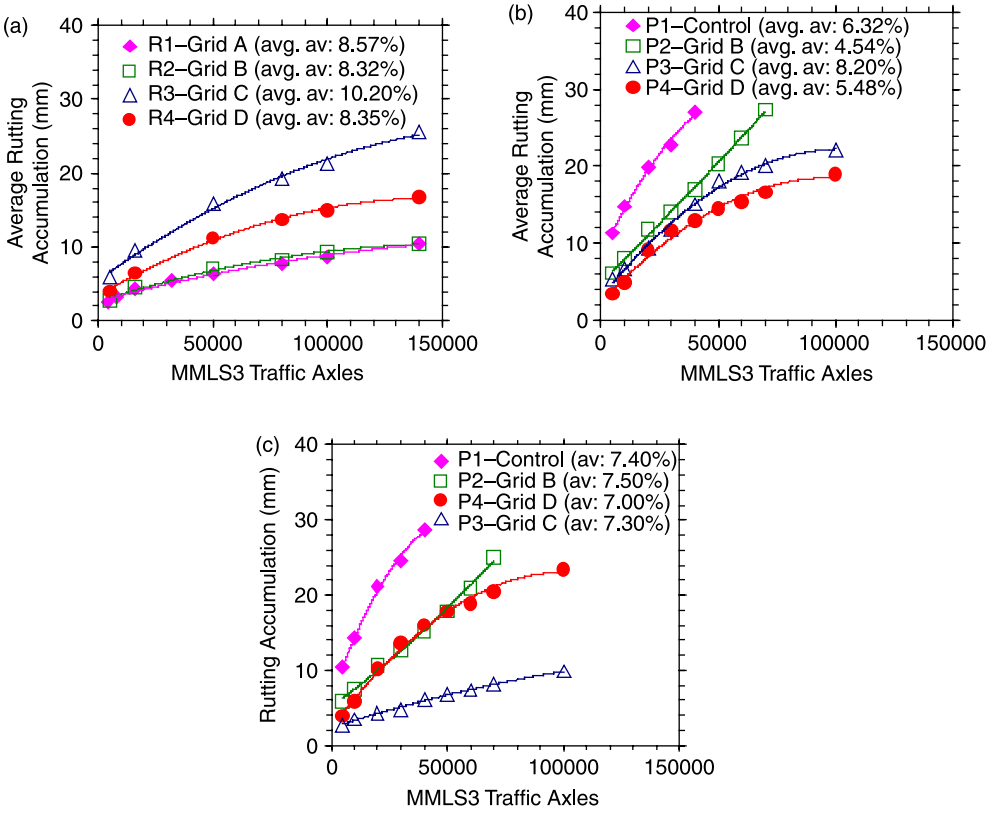

Figure 12. Rutting accumulation based on the average from all locations for each section: (a) APT I average rutting accumulation; (b) APT II average rutting accumulation and (c) APT II rutting accumulation for locations with similar asphalt mixture AVs.

of rutting performance between Grids B and D, although both are considered flexible grids.

While more replicates are necessary, particularly for different subgrade soil types, the measured rutting and observation from trenching provide evidence that the effectiveness of geogrid reinforcement and strengthening of weak subgrade is dependent on the interaction between the reinforcement and the surrounding materials. Thus, proper selection of the geogrid type for a given subgrade is essential. While a specific geogrid provides adequate support for a particular subgrade, it might not perform as well when used for a different type of soil and/or aggregate base. In the case of this study, the section with Grid B experiences significantly higher rate of rutting accumulation in APT II than in APT I, indicating that Grid B might not be suitable for reinforcing a subgrade as weak as that in APT II.

Due to the construction variability, sections in APT I exhibit overall higher asphalt AVs than that in APT II (Figure 10). Hence, the rutting measured at locations with similar AC AVs should be considered as points of direct

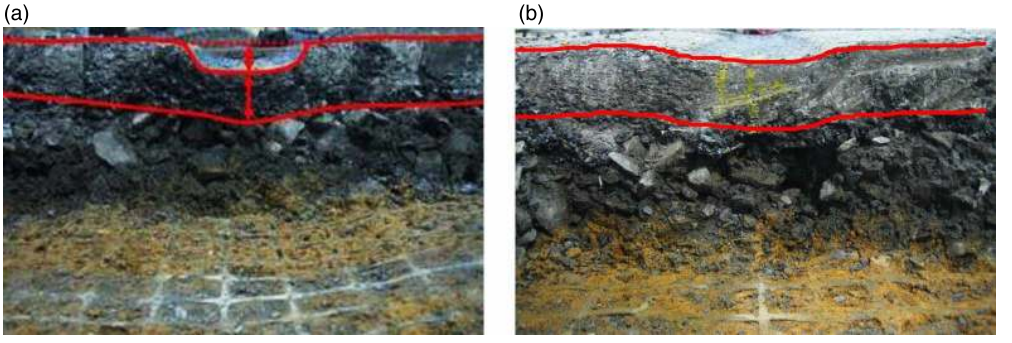

Figure 13. Trench cross-section of the pavement: (a) extensive deformation in APT I-R3 and (b) slight densification in the asphalt layer of APT I-R4.

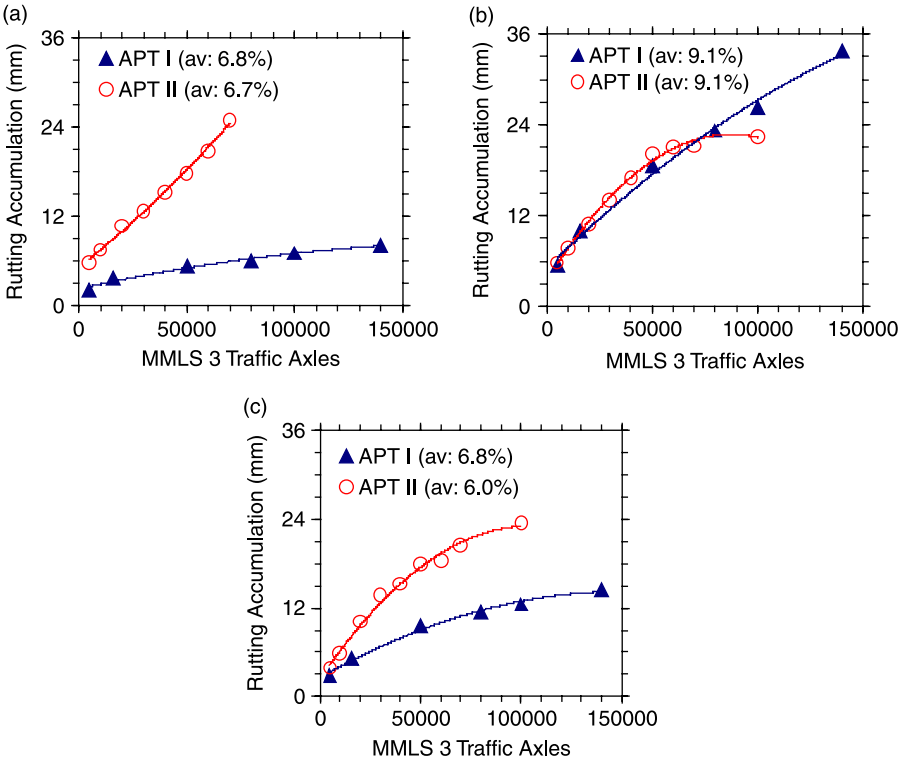

Figure 14. Rutting for geogrid reinforcement in APT I and APT II: (a) Grid B; (b) Grid C and (c) Grid D.

comparison. Figure 14 shows the comparison between the rutting of Geogrids B–D from the APTs I and II tests. The rutting resulting from APT II is greater than that of APT I for all geogrid types, given the weaker subgrade in APT II. Note, however, that the sections reinforced with Geogrid C exhibit very similar rutting in both the APTs I and II tests despite the difference in subgrade CBR. This indicates that Grid C is more effective in reinforcing weak subgrade compared to other geogrids used in this study.

4.2 Correlation between results of index and bench-scale testing

4.2.1 Index and direct shear test results

The shear resistance of the soil–geogrid–aggregate interface against direct sliding movement consists of geogrid's skin friction, soil–aggregate friction and passive resistance against the geogrid's transverse ribs. However, the contribution from the geogrid skin friction is likely to be minimal due to its relatively small surface area with respect to the total area of the interface. On the other hand, the area of the geogrid's aperture determines the contact surface between the subgrade soil and the aggregates from the base, thus affecting the overall soil–aggregate interface friction. Figure 15(a) illustrates the relationship between the interface efficiency factor (Equation (1)) and the aperture area. Geogrids with a larger aperture area result in higher interface efficiency factor for the types of materials used in this study. There is no correlation between the rib thickness and the interface efficiency factor. Both Grids B and C exhibit factors greater than 1.

The passive resistance exerted on the bearing members of the geogrid to some extent depends on the junction strength when considering the sliding movements against the ribs between junctions, and possibly tensile strength at small strains. The combination of the junction strength and the tensile strength at 2% strain in the machine direction has a strong correlation with the interface efficiency factor (Figure 15(b)). Junction thickness as the indictor of the junction strength also shows a good correlation with the interface efficiency factor (Figure 15(c)).

4.2.2 Index and pull-out test results

Determining the correlation between geogrid index properties and pull-out test results is evaluated through the coefficient of interaction. The coefficient of interaction, however, is calculated at a maximum pull-out force at the onset of failure. For pavement applications, it is more appropriate to investigate the effect of index properties on the behaviour of geogrids in the pull-out test at small displacements. The displacement experienced by the geogrids in pavement applications at the subgrade is much smaller than that resulting in other applications such as slope

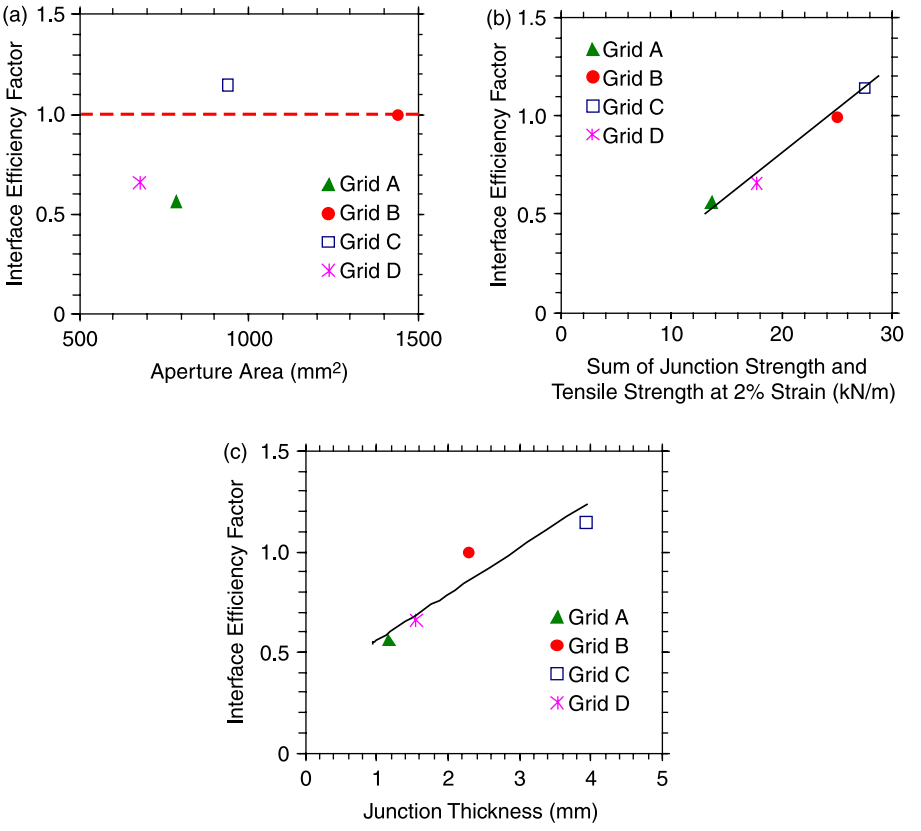

Figure 15. Correlation between E_ϕ (interface efficiency factor) and geogrid index properties: (a) aperture area; (b) sum of the junction strength and the tensile strength at 2% strain in the machine direction and (c) junction thickness.

stabilisation and retaining walls; moreover, a complete pull-out of the geogrid does not occur. Thus, for pavement applications, evaluating the load–displacement relationship at small displacements is more meaningful to the pull-out behaviour compared to the coefficient of interaction derived from a single value of the maximum pull-out load.

With regard to the fact that small strains in geosynthetics are typically developed for reinforced soil structure (McGown *et al.* 2005), it is more relevant to compare the geogrid's behaviour and interaction properties, such as in a pull-out test, at small displacements when they will be subjected to in the medium and under normal operational conditions. The displacements of the geogrids for subgrade stabilisation are expected to be minimal. Figure 16 shows the load–displacement relationship for the four geogrids up to 5 mm displacement. Due to limitations in instrumentation, unit displacements less than 0.3 mm cannot be measured. Figure 16 shows that within the first 5 mm of displacement, the slope of the pull-out force–displacement curves is nearly the same for all tested grids. Grid C exhibits the highest pull-out force at small displacements in spite of its low interaction coefficient (Table 3). Furthermore, the rankings in Figure 16 reveal a direct correlation with the friction angle and the efficiency factor from direct shear results, with the exception of Grid D.

Although the index properties of Grid D and its behaviour from direct shear test are comparable to other geogrids, particularly Grid A, it is highly likely that the significantly lower pull-out forces measured are due to experimental errors, and thus the pull-out results of Grid D can be considered as an anomaly. This proposition

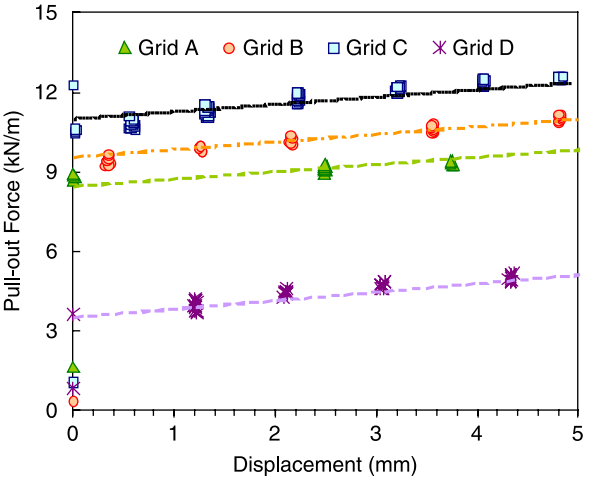

Figure 16. Pull-out force versus displacement for the various geogrid types at small displacements.

is confirmed by the fact that the average rutting for the section with Grid D is not as low as the pull-out force results suggest, and is actually less than that for all other sections in APT II (Figure 12(b)). Thus, Grid D will not be incorporated in the investigation of correlations linked to the pull-out force.

Figure 17 illustrates the correlation between the index properties and the pull-out force at 5 mm. It can be concluded that an insignificant correlation exists between the increase in aperture area and flexural rigidity and an increase in the pull-out force measured at 5 mm. Stronger correlations are observed for tensile strength at 2% strain and efficiency factor from direct shear.

Figure 18 shows that there is no evident correlation between the index properties and the coefficient of interaction. However, it is worth to further discuss the effect of the aperture area on the interaction coefficient. In order for effective interlocking of the aggregate–geogrid skeleton to take place, the ratio of aperture size to aggregate particle size should allow aggregates to strike through the aperture. Maximum interaction efforts can be achieved when the grain size is similar to that of the

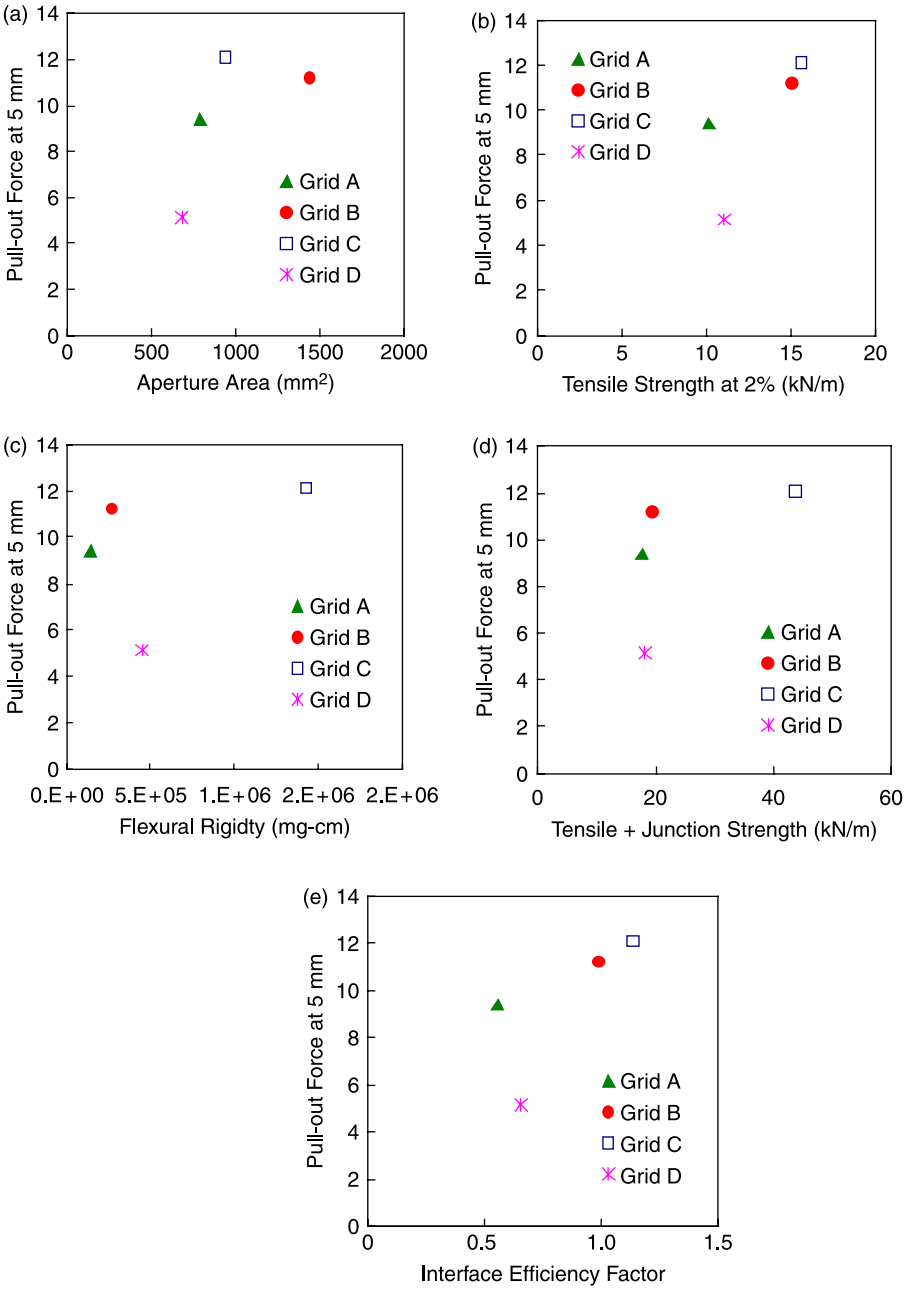

Figure 17. Effect of geogrid properties on the pull-out force measured at 5 mm displacement.

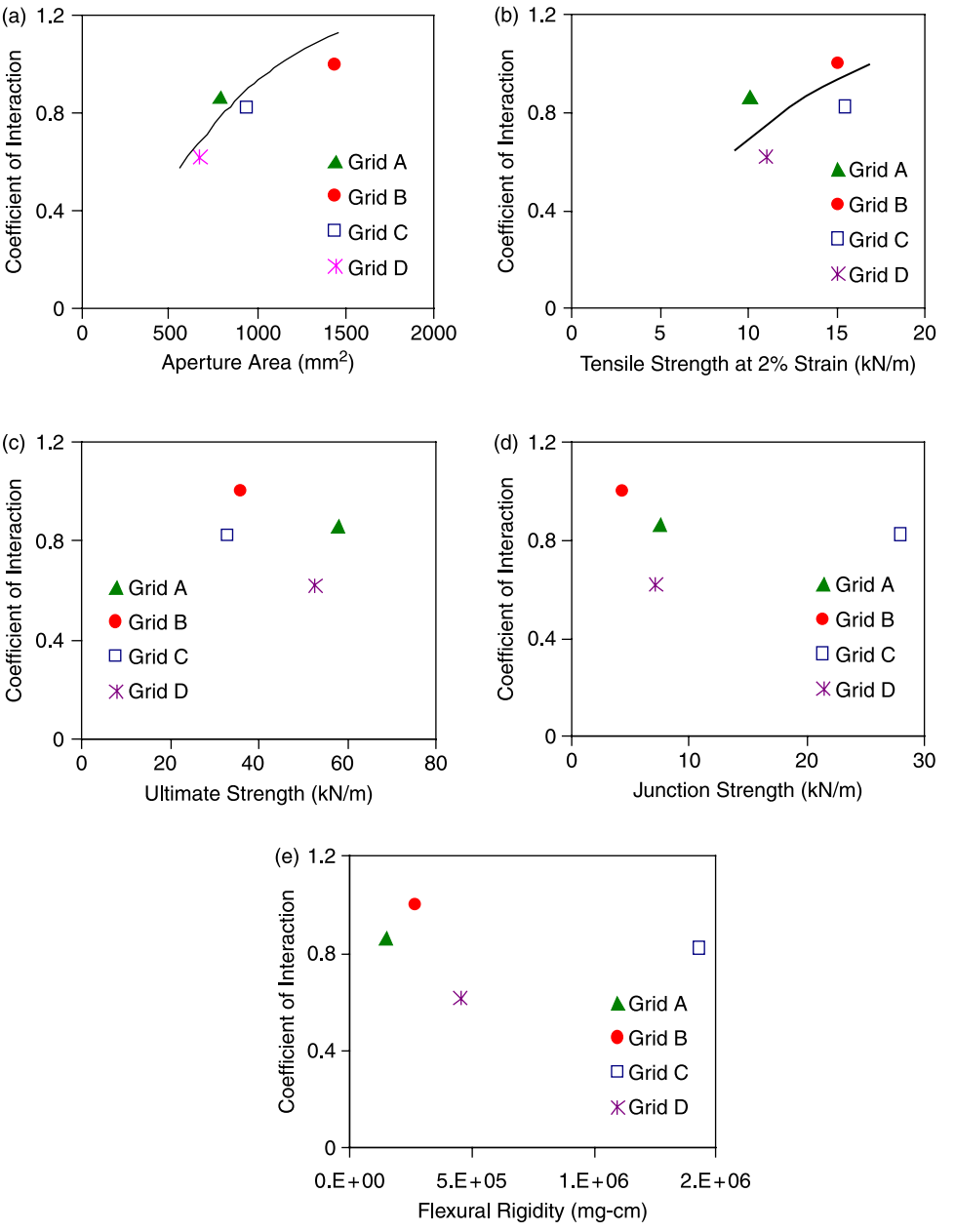

Figure 18. Correlation between index properties and coefficient of interaction.

geogrid aperture size (Shukla 2002). As can be seen in Table 2, the aperture sizes of Geogrids A–D are greater than 25.4 mm (1 in.). The course aggregate gradation suggests that ~87% of the material passes the 19 mm (0.75 in.) sieve. The surrounding material grain size distribution, relatively dense graded with nominal maximum aggregate size of 17.5 mm (1/2 in.), may positively impact that interlock. Grid B has the largest apertures among the other geogrid products used in this study (Table 2), which could partially explain its highest interaction coefficient, C_i (Equation (2)).

4.3 Correlation between index, bench-scale testing and accelerated testing results

Figure 19 shows the relationships between the geogrid bench-scale test results, namely the coefficient of interaction and the interface efficiency factor, and the measured subgrade rutting from the accelerated testing APTs I and II, while Figure 20 relates the geogrid index properties to the measured rutting. It is observed that the effects of ultimate strength, junction strength and bench-scale testing properties on measured rutting are not strongly evidenced, possibly due to the dominance of low

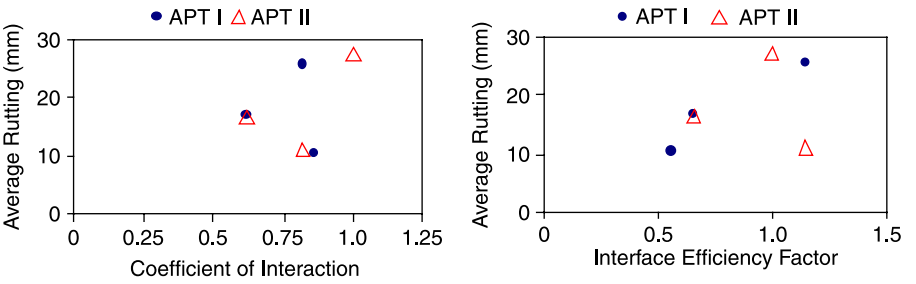

Figure 19. Correlation of mechanistic properties from bench-scale testing with average rutting from APT.

cyclic strains occurring in the geogrids at the subgrade level when compared to high strain levels applied under a monotonic loading condition until failure in index testing. In none of the accelerated testing runs are any of the geogrid samples stretched to a strain limit close to or at failure based on the observations of geogrids after trenching. This is in line with observations made from full-scale sections in the field (Perkins 1999).

Flexural rigidity and aperture area seem to affect the rutting according to trends that are dependent on the CBR. For the subgrade soil CBR of 3.0 in APT I, the general trend shows increased rutting with increases in aperture area and flexural rigidity. The trend is reversed for APT II, in which the subgrade soil CBR is 1.5.

The observations above do not offer conclusive correlations between some index properties, bench-scale

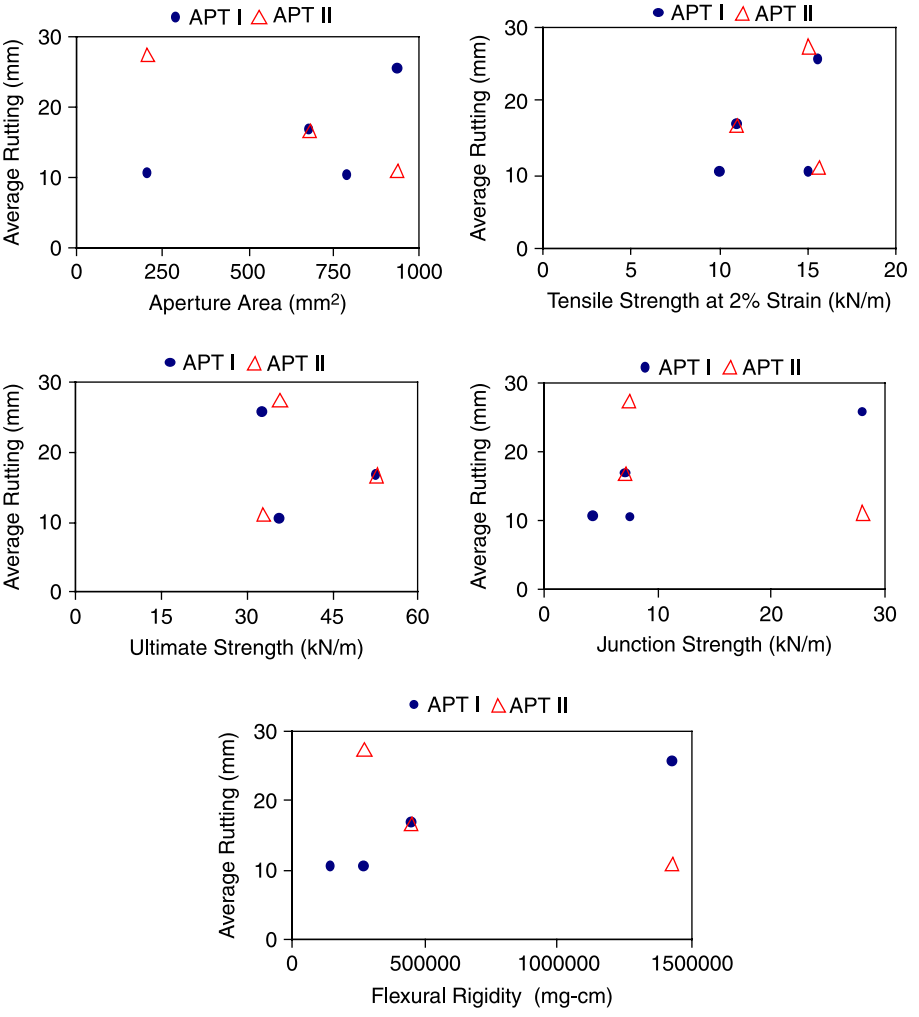

Figure 20. Correlation of geogrid properties from index testing with average rutting from APT.

Table 5. Relationship between selected index and bench-scale properties with subgrade rutting from accelerated testing.

Property	Correlation and observed trend				
	Efficiency factor	Pull-out @ 5 mm	Coefficient of interaction	Rutting @ 1.5 CBR	Rutting @ 3.0 CBR
Aperture area	I	I	I	D	I
Junction strength	I	I	N	D	I
Tensile strength at 2% strain	I	I	N	N	N
Ultimate strength	N	I	N	N	N
Flexural rigidity	N	I	N	D	I
Efficiency factor		I	N	N	I
Pull-out force @ 5 mm				N	N
Coefficient of interaction				N	N

I, increasing trend; D, decreasing trend; N, no observed trend.

testing properties and measured rutting under trafficking. More trials and replicates of APT need to be conducted to evaluate the statistical significance of any observed correlations and to assess the possibility of statistical interaction between the properties and their effects on rutting. Table 5 summarises the observed correlations among the index properties, bench-scale testing properties and measured rutting from the APT.

It should be noted that during the construction of the pavement sections for both the sets of APT, the sections that are reinforced with a stiff geogrid exhibited difficulty in achieving proper compaction of the asphalt layer. It is speculated that the high stiffness of the geogrid itself led to the insufficient compaction since the stiffness is the major difference between Grid C and other geogrids used in this study; nevertheless, care should be taken to ensure the proper construction of thin geogrid-reinforced pavements. Interpretations and any consequent conclusions presented here are based solely on the types of soil, geogrids, structural design and loading used in the two sets of APT.

5. Conclusions and recommendations

The objective of this study addresses the evaluation of geogrids for weak subgrade stabilisation. Evaluation is done through a spectrum of experiments ranging from index testing to determine physical properties of the geogrid, passing through bench-scale tests to understand the mechanical behaviour of the geogrids in an unbound medium, culminating in performance evaluation under accelerated traffic loading. Results from the various levels of testing are investigated to determine correlations between index properties, bench-scale testing and ultimately, the measured rutting under APT.

The interface efficiency factor parameter is used to evaluate the performance of geogrids in the direct shear tests. Tensile strength at 2% strain and junction strength contribute to the characterisation of geogrids in a complex manner, affecting the interaction properties of the reinforcement interface. A good correlation is found between combined geogrid tensile strength at 2% strain, junction strength and results of direct shear tests, while aperture opening does not show a strong correlation with the direct shear test results.

As another indicator of the effectiveness of using geogrids as reinforcing elements for subgrade stabilisation, the coefficient of interaction between the geogrid and the surrounding material is determined through pull-out tests. A strong correlation between aperture opening and interaction coefficient indicates that the aperture opening of the geogrid plays an important role in its interaction with the ABC materials. Although ultimate tensile strength and junction strength are not strongly correlated with the coefficient of interaction, they are expected to be important intrinsic properties of geogrids for gaining high pull-out resistance. Grid C with the highest junction strength shows the best pull-out resistance according to the relationship between the pull-out force and the telltale displacements.

The APTs I and II tests are conducted using the one-third scale MMLS3 on pavement sections with cross-sections scaled to one-third of actual pavement dimensions in the field. Pavement sections are constructed in a test pit and tested on two types of subgrade soils. For the APT I test, although, the lowest rutting is recorded for the section with the best interaction performance, it does not show strong consistency with bench-scale testing results, partially due to the variation in the AV content of the AC layer of that section. In the APT II test, rutting accumulation with the exclusion of asphalt AV variation demonstrates the substantial benefits of geogrid stabilisation for weak subgrade soil. Furthermore, a comparison of rutting performance differentiates the effectiveness of geogrid reinforcement for subgrade stabilisation among the three geogrid products in APT II. This difference is correlated with certain geogrid index properties and interaction characteristics through a correlation analysis. Aperture size, tensile strength at small strains, junction strength and flexural rigidity are recognised as the most important attributes of geogrids in pavement subgrade stabilisation.

By comparing the rutting behaviour among sections in the two sets of APT, certain geogrid products are found to be more suitable for use in conjunction with a stronger subgrade. It is therefore possible that geogrids that meet the criteria in physical and mechanical properties identified above will provide sufficient reinforcement for weak subgrade soils.

Observations and correlations made are limited to the two types of subgrade soils and one aggregate type used for subbase. A high number of variables exist in conducting the accelerated testing, including soil types, geogrid types, base layer aggregate gradation, moisture conditions and AVs of asphalt layers, among others. Important variables to consider include the extent of mixing between the subgrade soil and the base layer aggregates in addition to the exact location of the interface with respect to the geogrid after compaction. Thus, a wider scale study should be conducted, minimising these variables as much as possible and including instrumentation for displacement measurement within each layer, strain measurement on the geogrid and stress at the subgrade.

Notes

1. Email: xxt103@psu.edu
2. Email: angel.palomino@engr.psu.edu

References

Al-Qadi, I.L., *et al.*, 1994. Laboratory evaluation of geosynthetic-reinforced pavement sections. *Transportation Research Record 1439*, Washington, DC, 25–31.

Al-Qadi, I.L., *et al.*, 2007. Accelerated full-scale testing of geogrid-reinforced flexible pavements. *TRB 2007 Annual Meeting (CD-ROM)*. Washington, DC: Transportation Research Board, National Research Council.

Barksdale, R.D., Brown, S.F., and Chan, F., 1989. Potential benefits of geosynthetics in flexible pavement systems. *National Cooperative Highway Research Program (NCHRP) Report No. 315*. Washington, DC: Transportation Research Board, National Research Council.

Bergado, D.T. and Chai, J.-C., 1994. Pullout force/displacement relationship of extensible grid reinforcements. *Geotextile and Geomembrane*, 13, 295–316.

Chehab, G.R., Palomino, A.M., and Tang, X., 2007. Laboratory evaluation and specification development for geogrids for highway engineering applications. *Report No. FHWA-PA-2007-009-050110*.

Farrag, K., Acar, Y.B., and Juran, I., 1993. Pull-out resistance of geogrid reinforcements. *Geotextiles and Geomembranes*, 12 (2), 133–159.

Hass, R., Wall, J., and Carroll, R.G., 1988. Geogrid reinforcement of granular bases in flexible pavements. *Transportation Research Record 1188*. Washington, DC, 19–27.

Huang, Y.H., 2004. *Pavement analysis and design*. Upper Saddle River, NJ: Pearson Prentice Hall.

Hufenus, R., *et al.*, 2006. Full-scale field tests on geosynthetic reinforced unpaved roads on soft subgrade. *Geotextiles and Geomembranes*, 24 (1), 21–37.

Ingold, T.S., 1983. Laboratory pullout testing of grid reinforcements in sand. *Geotechnical Testing Journal*, 6 (3), 101–111.

Jewell, R.A., *et al.*, 1984. Interaction between soil and geogrids. *Proceedings of the conference on polymer grid reinforcement*. London: Thomas Telford, 18–30.

Juran, I., *et al.*, 1988. Pull-out response of geotextiles and geogrids (synthesis of available experimental data). *Proceedings of symposium on geotextiles for soil improvement*. ASCE, GSP No.18. Reston, VA: ASCE, 92–111.

Koerner, R.M., 1998. *Designing with geosynthetics*. 4th ed. New Jersey: Prentice Hall.

Love, J.P., 1984. *Model testing of geogrids in unpaved roads*. Dissertation (Doctoral). University of Oxford, Oxford, UK.

Martin, A.E., *et al.*, 2003. Pavement response and rutting for full-scale and scaled APT. *Journal of Transportation Engineering*, 129 (4), 451–461.

McGown, A., *et al.*, 2005. Testing biaxial geogrids for specification and design purposes. *GRI-18 Geosynthetics Research and Development in Progress*. Conference at GeoFrontiers, Reston, VA, ASCE.

Metcalf, J.B., 1996. Application of full-scale accelerated pavement testing. *NCHRP Synthesis of Highway Practice No. 235*. Washington, DC: Transportation Research Board, National Research Council.

Mohiuddin, A., 2003. *Analysis of laboratory and field pull-out tests of geosynthetics in clayer soils*. Thesis. Louisiana State University, Baton Rouge, Louisiana.

Perkins, S.S., 1999. Geosynthetic reinforcement of flexible pavements: laboratory based pavement test sections. *Report No. FHWA/MT-99-001/8138*. US Department of Transportation, Federal Highway Administration, Washington, DC.

Shukla, S.K., 2002. *Geosynthetics and their applications*. London: Thomas Telford.

Tatlisoz, N., Edil, T.B., and Benson, C.H., 1998. Interaction between reinforcing geosynthetics and soil-tire chip mixtures. *Journal of Geotechnical and Geoenvironmental Engineering*, 124 (11), 1109–1119.